Laboratory estimation of fracture compliance of a fluid-filled fracture using AVO response of a nonwelded interface

Minato, Shohei; Ghose, Ranajit

DOI
10.1190/segam2016-13840306.1

Publication date
2016

Document Version
Accepted author manuscript

Published in
SEG Technical Program Expanded Abstracts 2016

Laboratory estimation of fracture compliance of a fluid-filled fracture using AVO response of a nonwelded interface

Shohei Minato and Ranajit Ghose, Delft University of Technology*

SUMMARY

We explore the potential of multi-angle AVO inversion of P-P and P-S reflections from a fracture to estimate fracture properties. Although AVO analysis of welded interface like geological layer boundaries is common, the use of AVO variations for nonwelded boundaries like fractures is yet to be investigated. We conduct laboratory experiments to measure reflection responses of dry and wet fractures. The observed P-P reflections of the fracture and the fracture aperture are very well predicted by the nonwelded interface model. We invert the angle-dependent P-P reflectivity of the fracture to estimate both normal and tangential fracture compliances. The estimated value of the normal compliance is accurate, and it is also possible to obtain the value of the non-zero tangential compliance. We find that supplementing the information of converted P-S reflections in the AVO inversion greatly improves the estimate of the tangential compliance. The calculated compliance ratio clearly shows the existence of fluid in the fracture. This finding can be crucial for new applications in a wide range of scale - from earthquake seismology, deep and shallow seismic exploration, to nondestructive material testing.

INTRODUCTION

A nonwelded interface is a boundary across which traction is continuous but seismic displacement is discontinuous (e.g., Schoenberg, 1980). The nonwelded interface is characterized by its elastic compliance which relates the seismic-displacement jump with the seismic traction. The model is found to be useful to represent a thin, compliant zone in a material, e.g., fractures in rocks (Nagy, 1992).

Depending on the seismic wavelength used, fractures can be regarded as various thin, compliant zones in rocks, in different scales. For example, in laboratory-scale experiments, reflection and transmission coefficients are used to characterize the compliances of natural fractures (e.g., Pyrak-Nolte et al., 1990; Lubbe et al., 2008) and to monitor the frictional strength of rough solid surfaces (Nagata et al., 2008). In field-scale seismic measurements, the concept of reflection/transmission response from a nonwelded interface is useful to study large fractures such as rock joints (e.g, Cook, 1992; Li et al., 2014). The concept is also applicable to macroscopic faults: Worthington and Hudson (2000) discussed the use of nonwelded interfaces to predict VSP responses of geological faults and Kame et al. (2014) discussed the feasibility of this concept to monitor earthquake cycle at a plate boundary.

In this study, we consider a plane-wave reflection problem of a nonwelded interface: we consider elastic waves which have a wavelength that is larger than the thickness of a fracture and also larger than the spacing between the asperities of contact, but shorter than the lateral extent of the fracture (Gu et al., 1996; Pyrak-Nolte and Morris, 2000).

Though well-known for layer boundaries (i.e., welded interfaces), the AVO response of a nonwelded interface has not been utilized so far to estimate fracture compliances. This is mainly because of the lack of high-frequency components in the conventional exploration-scale seismic experiments, which cannot resolve sufficiently the reflections from a single fracture. However, recent developments in microseismic observation using boreholes have enabled successful field measurement of relatively high-frequency reflections from a single fracture (Reshetnikov et al., 2010). The majority of the earlier laboratory-scale fracture experiments has considered only normally incident seismic waves (e.g., Pyrak-Nolte et al., 1990; Lubbe et al., 2008) and a few earlier studies that have considered oblique incidence at a nonwelded interface are especially for nondestructive material testing (e.g., Margetan et al., 1988; Liaptsis et al., 2006; Nam et al., 2012), where multiple incidence angles at a given point on the interface were not utilized in the inversion.

In this study, we consider P-P and P-S AVO variations at a nonwelded interface. The use of the multiple oblique incidence waves offers a new possibility for simultaneous and robust estimation of both normal and tangential compliances (η_N and η_T). Estimating the compliance ratio is especially useful for predicting the existence of fluid in the fracture (e.g., Bakulin et al., 2000; Lubbe et al., 2008). This estimation using only a P-wave source was not possible before. An obliquely incident P-wave also produces the converted P-S wave at the nonwelded interface. The P-S reflection coefficient is sensitive to η_T (Chaisri and Krebes, 2000), thus promising to provide an estimate of η_T.

We measured the P-P and P-S AVO responses from a fracture in the laboratory. At first, we calculated the reflection coefficient of a water-filled fracture using the dry fracture response as the reference. We then checked the efficacy of the nonwelded interface representation of the angle-dependent reflection responses. Finally, we explored the possibility and accuracy of multi-angle AVO inversion for η_N and η_T from the measured angle-dependent P-P and P-S reflection coefficients at the fracture.

NONWELDED INTERFACE

The boundary condition of a nonwelded interface can be written as,

$$\Delta\mathbf{u} \quad = \quad \mathbf{Z}\mathbf{t}, \tag{1}$$

where $\Delta\mathbf{u}$ and $\mathbf{t}$ are, respectively, the jump in the seismic displacement vector across the fracture interface and the traction vector in the fracture-oriented Cartesian coordinate. Assuming

a rotationally invariant compliance matrix (Schoenberg, 1980), the fracture compliance matrix $\mathbf{Z}$ consists of η_N and η_T as $\mathbf{Z} = \mathrm{diag}(\eta_T, \eta_T, \eta_N)$.

In the following experiment, we consider the fracture as a thin, parallel-wall layer filled with a soft material which is often used to represent hydraulic fractures (e.g., Fehler, 1982; Groenenboom and Fokkema, 1998). In this case, the fracture compliance can be represented as (e.g., Baik and Thompson, 1984; Liu et al., 2000):

$$\eta_N = \frac{\Delta}{\lambda' + 2\mu'}, \quad (2)$$

$$\eta_T = \frac{\Delta}{\mu'}, \quad (3)$$

where μ' and λ' are the Lamé constants of the fracture infill, and Δ is the aperture of the fracture. Note that the nonwelded interface representation and the application of the AVO inversion that we discuss in this study are not limited to the thin, parallel-wall layer model (equation 2 and 3). Assuming a model with randomly distributed asperities and an effective aperture, η_N and η_T are found to be the functions of the asperity distribution, fracture aperture and infill materials (Worthington and Lubbe, 2007). The review of various fracture models using a nonwelded interface can be found in Liu et al. (2000).

THEORETICAL REFLECTION COEFFICIENTS

The explicit form of P- and SV-wave reflection coefficients due to incident P-wave on a nonwelded interface within a homogeneous medium were derived earlier (Chaisri and Krebes, 2000):

$$R_{PP} = \left[\omega^2 \eta_N \eta_T KL + 2i\omega\rho\eta\left(\eta_N\gamma^2 - \eta_T\chi^2\xi^2\right)\right] D^{-1}, \quad (4)$$

$$R_{PS} = -2\gamma\chi\xi\frac{V_P}{V_S}\left[\omega^2\eta_N\eta_T K + i\omega\rho\left(\eta_T\xi + \eta_N\eta\right)\right] D^{-1}, \quad (5)$$

where,

$$D = (2\rho\xi - i\omega\eta_N K)(2\rho\eta - i\omega\eta_T K), \quad (6)$$

$$\chi = 2\rho V_S^2 p, \gamma = \rho(1 - 2V_S^2 p^2), \quad (7)$$

$$\xi = \frac{\cos\theta_{PP}}{V_P}, \eta = \frac{\cos\theta_{PS}}{V_S}, \quad (8)$$

$$K = \gamma^2 + \chi^2\xi\eta, L = \gamma^2 - \chi^2\xi\eta. \quad (9)$$

Here p is the ray parameter ($p = \sin\theta_{PP}/V_P$) and θ_{PS} is the angle of reflected S-wave.

EXPERIMENT SETUP

Our experimental setup consists of two aluminum blocks with parallel and smooth surfaces (Figure 1). We assume that the aluminum block is homogeneous and isotropic (V_P = 6380 m/s, V_S = 3150 m/s and ρ = 2700 kg/m^3). An artificial horizontal fracture is simulated by installing spacers of known thickness (100 μm) between the two blocks. We installed seven longitudinal transducers (Panametrics V103) for an array-seismic measurement (one transmitter and six receivers). The spacing between the transducers is 3.5 cm: we obtain six incidence angles for both P-P reflections (5.8°, 11.5°, 17.0°, 22.1°, 27.0° and 31.4°) and P-S reflections (7.8°, 15.4°, 22.6°, 29.4°, 35.6° and 41.2°). We generated source signals (truncated sinusoid) with 1.0 MHz center frequency.

We measured the reflection responses as follows. We assemble the two blocks with a spacer between them to simulate an air-filled (dry) fracture. After we measure the reflection responses of the dry fracture, we carefully lift the top block so that the receiver coupling does not change, and we put a mixture of water and hair gel on the surface between the blocks. Then we lower the top block to the original position in order to simulate a water-filled (wet) fracture and measure the reflection responses again. Note that the fluid with a vanishingly small shear modulus results in a vanishingly small tangential stiffness of the fracture (η_T^{-1}, see equation 3).

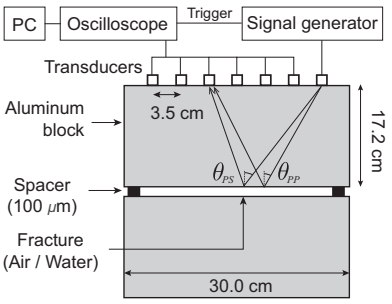

Figure 1: Experimental setup for measuring angle-dependent reflections from a fracture

ESTIMATION OF NORMAL COMPLIANCE FROM P-P AVO INVERSION

We checked the efficacy of the nonwelded interface representation of angle-dependent reflection responses for the water-filled fracture by first estimating η_N at various incidence angles for the P-P reflections and then calculating the effective fracture aperture by assuming the tangential fracture stiffness (η_T^{-1}) to be zero.

We observed the P-P reflections for the dry and the wet fracture at the receiver array (six incidence angles) after bandpass (0.01 MHz–1.8 MHz) filtering and muting around the P-P reflections (Figure 2). We assume that the difference between the dry and the wet fracture response is only in the reflection coefficients at the fracture and that the incident waves at the fracture and the effect of propagation (e.g., geometrical spreading and attenuation) between the source and receivers are identical between dry and wet conditions. Because the dry fracture responses are equivalent to the free-surface ones, we calculate the angle- and frequency-dependent P-P reflection coefficient of the wet fracture ($R_{PP}^{Wet}(\omega, \theta_{PP})$) using the following relation:

$$R_{PP}^{Wet}(\omega, \theta_{PP}) = R_{PP}^{FS}(\theta_{PP})\frac{D^{Wet}(\omega, \theta_{PP})}{D^{Dry}(\omega, \theta_{PP})}, \quad (10)$$

where R_{PP}^{FS} is the theoretical free-surface P-P reflection coefficients (e.g., Aki and Richards, 2002). D^{Wet} and D^{Dry} are the P-P reflection responses for the wet and the dry fracture, respectively.

The reflection coefficient of the wet fracture is estimated using a least square fitting of the observed coefficients with the theoretical P-P reflection coefficients for a nonwelded interface (equation 4) as a function of η_N. The estimated reflection coefficient clearly demonstrates an AVO effect for the nonwelded interface (Figure 3a). The estimated values of η_N at different incidence angles are summarized in Figure 3(b). Finally, the predicted waveforms of the wet fracture using the estimated values of η_N match quite well with the observed angle-dependent reflection responses (red lines in Figure 2b).

Using the value of the bulk modulus of water (2.2 GPa), we estimated the effective aperture of the fluid-filled fracture from η_N, using equation 2. The estimated apertures are larger than the installed spacer thickness (see red lines in Figure 3b) because a residual aperture is effectively created due to the dents and scratches on the surface of the aluminum blocks. To evaluate this residual aperture, we performed the same procedure described in the previous subsection again but without installing the spacer. We find that the average residual aperture is 42 μm over all receivers (blue dotted line in Figure 3b).

When we compare the estimated values of the fracture aperture with the true aperture value (i.e., spacer thickness + residual aperture), we find that the nonwelded interface model estimates reasonably well the fracture aperture for all incidence angles (red lines in Figure 3b).

P-P AND P-S JOINT AVO INVERSION

In the previous section we assume that we have prior information that the fracture does not have asperities with zero tangential fracture stiffness (η_T^{-1}). In this section we assume that we do not have such prior information about the structure of the fracture and the material in the fracture. We then discuss the possibility of estimating simultaneously both η_N and η_T using P-P and P-S AVO responses.

Note that the true value of η_T is very large and cannot be resolved accurately in this experiment for the fracture scale and the frequency range that we use. This is because the reflection coefficients (equation 4 and 5) are insensitive to the large values of η_T. However, the computed misfit of the observed reflection coefficients provides the possible lowest-value of η_T, which is a crucial information in order to infer the structure of the fracture. We further estimated compliance ratio (η_N/η_T) in order to discuss the existence of fluids in the fracture (e.g., Bakulin et al., 2000; Lubbe et al., 2008). The AVO inversion offers the possibility of estimating the compliance ratio without using a S-wave source, which was not possible before.

We assume here the fracture compliances to be spatially constant along the fracture plane. The approach can, however, handle heterogeneous fracture compliances through processing of each common-mid-point (CMP) gathers. Recently scat-

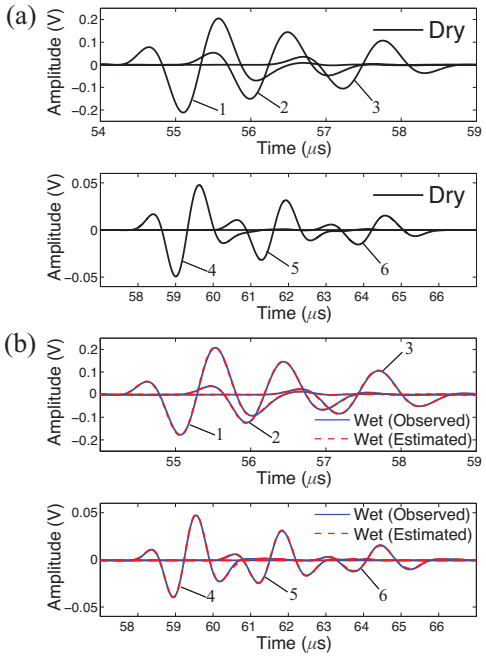

Figure 2: Observed angle-dependent P-P reflection responses (solid line) for (a) dry fracture and (b) water-filled fracture. The wet-fracture response is estimated (dashed line) using the observed dry fracture response and the nonwelded interface model. The estimated normal compliances are shown in Figure 3(b). The incident angles (θ_{PP}) are (1) 5.8°, (2) 11.5°, (3) 17.0°, (4) 22.1°, (5) 27.0° and (6) 31.4°.

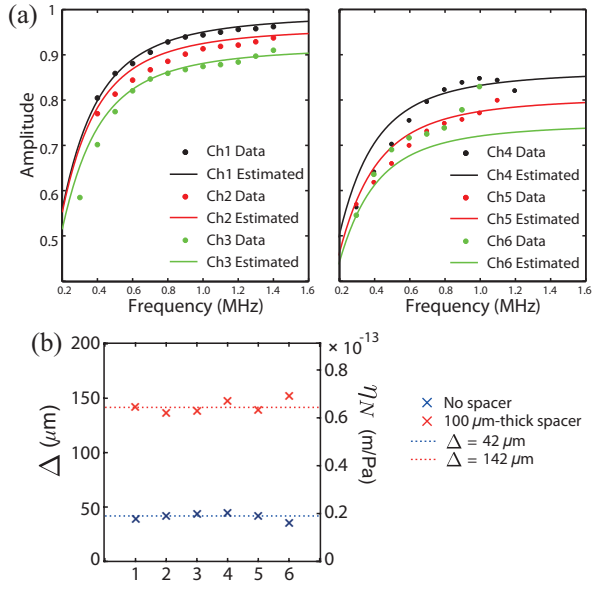

Figure 3: (a) Observed and estimated P-P reflection coefficients of the wet fracture using the least-square inversion. (b) Estimated normal compliances (η_N) and the fracture aperture (Δ). The horizontal axis presents the 6 incidence angles (θ_{PP}, see the caption of Figure 2). The true aperture (red dotted line) is obtained as the spacer thickness plus the residual aperture (42 μm), described in the text.

tered elastic waves have been used to characterize heterogeneous fracture compliances (e.g., Leiderman et al., 2007; Minato and Ghose, 2013, 2014).

We first consider only P-P reflections (Figure 2). We performed the same procedure as in the previous section to obtain the observed reflection coefficients (Figure 3a). We then estimated η_N and η_T by minimizing the misfit between the observed and the estimated reflection coefficients for all incidence angles simultaneously. The normalized misfit function S is defined as,

$$S(\eta_N,\eta_T)=\frac{\sqrt{\sum_{i,j}\left|R_{PP}^{obs}(\omega_i,\theta_j)-R_{PP}^{est}(\omega_i,\theta_j,\eta_N,\eta_T)\right|^2}}{\sqrt{\sum_{i,j}\left|R_{PP}^{obs}(\omega_i,\theta_j)\right|^2}}, \quad (11)$$

where $R_{PP}^{obs}(\omega_i,\theta_j)$ and $R_{PP}^{est}(\omega_i,\theta_j)$ are, respectively, the observed and the estimated P-P reflection coefficients for the $j-$th incident angle and the $i-$th frequency component.

We calculated the misfit function considering the range of the compliances to be $10^{-14}\leq\eta_N\leq10^{-12}$ and $10^{-14}\leq\eta_T\leq10^{-11}$. We discretized the compliance ranges in 400×400 samples and calculated the normalized misfit function (Figure 4a). Notice that we considered the upper bound of η_T to be 10^{-11} m/Pa because in the given frequency range we hardly see any changes in the theoretical P-P reflection coefficients and in the corresponding $S(\eta_N,\eta_T)$ for values of η_T larger than 10^{-11} m/Pa. The misfit function shows that η_N is more sensitive than η_T (Figure 4a). Furthermore, it illustrates that the estimated η_T is of the same order of magnitude or larger than η_N. The estimated minimum misfit in the inversion is located at $(\eta_N,\eta_T)=(6.34\times10^{-14},1.30\times10^{-12})$. Therefore, we obtain an accurate estimate of η_N (see Figure 3b for the true value). Due to the small sensitivity of η_T to the P-P reflection coefficient, however, the compliance ratio η_N/η_T (a fluid indicator) is detected as 0.48. Unfortunately, this value of compliance ratio is too large for a wet natural fracture created in a laboratory experiment (Lubbe et al., 2008), which implies that this can be misinterpreted as a dry natural fracture. Nevertheless, Figure 4(a) shows that we can detect the possible lowest-value of non-zero η_T from multi-angle P-P AVO inversion. In our experiment, we have a maximum incidence angle of 31.4°. The use of higher incidence angles will improve the sensitivity to η_T, as shown in Chaisri and Krebes (2000).

We introduced the P-S reflections in the inversion procedure described above. The similar procedure was applied to calculate the P-S reflection coefficients (equation 5) for the wet fracture. The calculated P-P and P-S reflection coefficients were then simultaneously inverted to estimate η_N and η_T.

The calculated misfit function (Figure 4b) shows that the sensitivity to η_T is now greatly improved from the one using only P-P reflections (Figure 4a). The estimated minimum misfit is located at $(\eta_N,\eta_T)=(6.41\times10^{-14},1.00\times10^{-11})$. Note that η_T is estimated to be at the upper bound of the range: η_T is found to be at least two orders of magnitude larger than η_N. The resulting compliance ratio is shown to be 0.064, which can be unambiguously interpreted as a wet fracture (Lubbe et al., 2008).

Note that although our situation is not same as that of a natural fracture containing asperities, the estimated values of η_N are similar to those of natural fractures (Lubbe et al., 2008). Furthermore, because of the large value of η_T, we obtain the possible lowest value for η_T. However, laboratory experiments using natural fractures show that η_T of a dry/wet fracture is of the same order of magnitude as η_N (Lubbe et al., 2008). Therefore, we expect to obtain more accurate values of η_T for natural fractures using the AVO inversion developed in this study, although it will require additional laboratory verification.

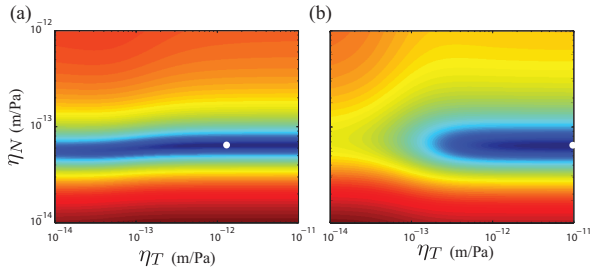

Figure 4: The misfit function in (a) multi-angle P-P AVO inversion and (b) joint P-P + P-S AVO inversion.

CONCLUSION

We conducted ultrasonic laboratory experiments to measure P-P and P-S AVO responses from a nonwelded interface (a dry and wet fractures) using aluminum blocks and spacers with known thickness. We estimated the reflection response of the wet fracture using the observed dry fracture response as a reference. By estimating the normal compliance and corresponding fracture aperture, we confirmed that the nonwelded interface model for a fluid-filled fracture describes quite well the angle-dependent P-P reflection responses, which indicates that the measurement using a long seismic wavelength (approximately 6 mm) correctly handles the reflections from a very thin (approximately 0.15 mm) layer.

Furthermore, we found that both normal and tangential compliances can be estimated from the multi-angle P-P AVO inversion. Our results showed that the normal compliance can accurately be obtained and that it is possible to estimate also the non-zero tangential compliance. Finally, we found that a joint inversion of P-P and P-S AVO responses greatly improves the estimation of the tangential compliance. The derived normal to tangential compliance ratio clearly showed the existence of fluid in the fracture, a finding that has a major application potential in wide ranges of scale and discipline.

ACKNOWLEDGMENTS

This work is supported by The Netherlands Research Centre for Integrated Solid Earth Science. We thank Karel Heller for his assistances in laboratory experiments.

REFERENCES

Aki, K., and P. G. Richards, 2002, Quantitative seismology second edition: University Science Books.

Baik, J., and R. B. Thompson, 1984, Ultrasonic scattering from imperfect interfaces: a quasi-static model: Journal of Nondestructive Evaluation, **4**, 177–196.

Bakulin, A., V. Grechka, and I. Tsvankin, 2000, Estimation of fracture parameters from reflection seismic data–part I: HTI model due to a single fracture set: GEOPHYSICS, **65**, 1788–1802.

Chaisri, S., and E. S. Krebes, 2000, Exact and approximate formulas for P-SV reflection and transmission coefficients for a nonwelded contact interface: Journal of Geophysical Research: Solid Earth, **105**, 28045–28054.

Cook, N., 1992, Natural joints in rock: Mechanical, hydraulic and seismic behaviour and properties under normal stress: International Journal of Rock Mechanics and Mining Sciences & Geomechanics Abstracts, **29**, 198–223.

Fehler, M., 1982, Interaction of seismic waves with a viscous liquid layer: Bulletin of the Seismological Society of America, **72**, 55–72.

Groenenboom, J., and J. T. Fokkema, 1998, Monitoring the width of hydraulic fractures with acoustic waves: Geophysics, **63**, 139–148.

Gu, B., R. Suárez-Rivera, K. T. Nihei, and L. R. Myer, 1996, Incidence of plane waves upon a fracture: Journal of Geophysical Research, **101**, 25337–25346.

Kame, N., K. Nagata, M. Nakatani, and T. Kusakabe, 2014, Feasibility of acoustic monitoring of strength drop precursory to earthquake occurrence: Earth, Planets and Space, **66**, 1–12.

Leiderman, R., P. E. Barbone, and A. M. B. Braga, 2007, Reconstructing the adhesion stiffness distribution in a laminated elastic plate: Exact and approximate inverse scattering solutions: The Journal of the Acoustical Society of America, **122**, 1906–1916.

Li, J., H. Li, Y. Jiao, Y. Liu, X. Xia, and C. Yu, 2014, Analysis for oblique wave propagation across filled joints based on thin-layer interface model: Journal of Applied Geophysics, **102**, 39–46.

Liaptsis, D., B. Drinkwater, and R. Thomas, 2006, The interaction of oblique incidence ultrasound with rough, partially contacting interfaces: Nondestructive Testing and Evaluation, **21**, 109–121.

Liu, E., J. Hudson, and T. Pointer, 2000, Equivalent medium representation of fractured rock: Journal of Geophysical Research, **105**, 2981–3000.

Lubbe, R., J. Sothcott, M. Worthington, and C. McCann, 2008, Laboratory estimates of normal and shear fracture compliance: Geophysical Prospecting, **56**, 239–247.

Margetan, F., R. Thompson, and T. Gray, 1988, Interfacial spring model for ultrasonic interactions with imperfect interfaces: Theory of oblique incidence and application to diffusion-bonded butt joints: Journal of Nondestructive Evaluation, **7**, 131–152.

Minato, S., and R. Ghose, 2013, Inverse scattering solution for the spatially heterogeneous compliance of a single fracture: Geophysical Journal International, **195**, 1878–1891.

———, 2014, Imaging and characterization of a subhorizontal non-welded interface from point source elastic scattering response: Geophysical Journal International, **197**, 1090–1095.

Nagata, K., M. Nakatani, and S. Yoshida, 2008, Monitoring frictional strength with acoustic wave transmission: Geophysical Research Letters, **35**, (L06310).

Nagy, P., 1992, Ultrasonic classification of imperfect interfaces: Journal of Nondestructive Evaluation, **11**, 127–139.

Nam, T., T. Lee, C. Kim, K.-Y. Jhang, and N. Kim, 2012, Harmonic generation of an obliquely incident ultrasonic wave in solid–solid contact interfaces: Ultrasonics, **52**, 778–783.

Pyrak-Nolte, L., and J. Morris, 2000, Single fractures under normal stress: The relation between fracture specific stiffness and fluid flow: International Journal of Rock Mechanics and Mining Sciences, **37**, 245–262.

Pyrak-Nolte, L., L. Myer, and N. Cook, 1990, Transmission of seismic waves across single natural fractures: Journal of Geophysical Research, **95**, 8617–8638.

Reshetnikov, A., S. Buske, and S. Shapiro, 2010, Seismic imaging using microseismic events: Results from the san andreas fault system at safod: Journal of Geophysical Research: Solid Earth, **115**, B12324.

Schoenberg, M., 1980, Elastic wave behavior across linear slip interfaces: The Journal of the Acoustical Society of America, **68**, 1516–1521.

Worthington, M., and R. Lubbe, 2007, The scaling of fracture compliance: Geological Society, London, Special Publications, **270**, 73–82.

Worthington, M. H., and J. A. Hudson, 2000, Fault properties from seismic Q: Geophysical Journal International, **143**, 937–944.